Chapter 7
Growth of One-Dimensional Nanomaterials in the ETEM

Jonathan Winterstein and Renu Sharma

Abstract One-dimensional nanomaterials (nanowires and nanotubes) have a number of unique and interesting properties that have made them the subject of significant research for a wide range of applications. Electron microscopy is generally necessary for their morphological, structural, and chemical characterization due to their small dimensions. For applications such as nanomanufacturing, the synthesis process must be scalable. In the case of nanoelectronics, the tolerances are demanding, necessitating stringent control of process parameters. Catalytic chemical vapor deposition (CVD) is currently the most suitable route that allows both scalable production and selective, aligned growth directly on a substrate. Characterization of growth parameters and atomistic growth mechanisms is necessary if such nanomaterials are to be engineered for specific applications. Environmental transmission or scanning transmission electron microscopy (ETEM or ESTEM) provides the needed platform for in situ monitoring of the influence of processing parameters on nanomaterial structure and morphology. In this chapter, we present the practical aspects of experiment design, data analysis, successful examples, and the limitations of the ETEM platform for following one-dimensional nanomaterial growth processes.

7.1 Motivation and Background

1D Nanomaterials, such as nanowires and nanotubes, are a class of materials with large aspect ratios (ratio of length to diameter) and absolute diameter dimensions below approximately 100 nm. The unique and interesting phenomena observed in these materials arise due to quantum confinement effects, high surface-area-to-volume ratios, and the absence of defects result in exceptional properties.

There are a wide range of applications that take advantage of these unique properties of 1D materials. For example, nanowires (NWs) have been proposed for use in electronic devices (Yang 2005), photonic devices (Reimer et al. 2012),

J. Winterstein (✉) • R. Sharma
Nanofabrication Research Group, Center for Nanoscale Science and Technology, NIST, Gaithersburg, MD, USA
e-mail: Jonathan.Winterstein@nist.gov; renu.sharma@nist.gov

T.W. Hansen, J.B. Wagner (eds.), *Controlled Atmosphere Transmission Electron Microscopy*, DOI 10.1007/978-3-319-22988-1_7

photovoltaics, thermoelectrics (Hochbaum and Yang 2009), chemical sensors (Cui et al. 2001), catalysts, and catalyst supports (Wang et al. 2011) and recently, in the case of Si NWs, as battery electrodes for Li-ion batteries, with intriguing results (Chan et al. 2008). In many instances, to maximize the effectiveness of NWs in a specific application, it is necessary to control the growth rate and direction, and the presence and arrangement defects. The single-crystal nature of many NWs is a particularly valuable feature, which is most easily confirmed with diffraction and imaging in an electron microscope.

Nanotubes constitute a second subset of 1D materials. They differ from nanowires as they are hollow instead of solid, with an individual single-walled carbon nanotube (SWCNT)—a single sheet of carbon atoms, a graphene sheet, rolled into a tube—being the canonical example. Moreover, the structural variation in nanotubes is not limited to different aspect ratios or diameters but includes the fact that their wall thickness, i.e., the number of concentrically rolled sheets can vary from a single sheet to multiple sheets. Carbon nanotubes (CNTs) were first identified by Iijima (1991) using high-resolution transmission electron microscopy (TEM) and electron diffraction. Applications for CNTs include field-emission electron sources for displays or high-brightness electron guns, high-strength composites, transparent electrodes, high-efficiency filters, and electronics, among many others. A tremendous amount of research has therefore been performed to understand and exploit the unique electrical, thermal, and mechanical properties of CNTs (Baughman et al. 2002; Robertson 2004; Meyyappan 2005; Dresselhaus et al. 2001).

The properties of nanowires and nanotubes are strongly dependent on their crystallography and morphology. The primary goal is thus the controlled synthesis of 1D structures with the required structure and dimensions to deliver the desired properties. The transmission electron microscope is now capable of obtaining direct, atomic resolution images of crystals and their defects. Chemical composition can also be mapped with a spatial resolution below the interatomic spacing in many materials. However, the ex situ information thus obtained is often not sufficient to optimize the synthesis conditions to yield the required structure and morphology. In situ measurements that reveal the effect of synthesis parameters on nucleation and growth mechanisms, structure and morphology, are therefore the subject of intense development efforts (Ross 2010; Sharma 2005).

Environmental TEM (ETEM) is an excellent tool for growth studies because it combines synthesis with characterization capabilities. With one experiment, the crystallography, morphology, defect structure, and chemical composition can be monitored during growth with moderate temporal resolution, which now reaches into the millisecond regime. Critical measurements such as growth rates are possible with atomic-scale accuracy. Importantly, ETEM offers the possibility of measuring the growth rate of individual nanomaterials and determining the structure and chemistry of the active nanoparticle catalysts. Although the wealth of information available from ETEM experiments has improved our understanding of nanomaterial growth and enabled new science and engineering, ETEM also has a

number of limitations that must be considered during experimental design and interpretation of results (Sharma 2005, 2012; Egerton et al. 2004).

In this chapter, we will review 1D nanomaterial growth with a focus on the fundamental phenomena that can be studied in the ETEM, followed by a practical description of experimental design, the important instrumental features, sample preparation, and data analysis. We will also review examples from the literature of successful ETEM growth experiments and the scientific knowledge gained. Finally, we discuss limitations, such as beam damage and uncertainties in temperature measurement, as these must be understood for correct interpretation of ETEM results.

7.2 CVD Synthesis Process

Chemical vapor deposition (CVD) is the most widely used method for the synthesis of 1D nanomaterials because it permits growth at relatively low temperatures with a high yield and the possibility of control over growth by selection of suitable catalysts, supports, temperature, and precursor pressure. In the CVD process, metal nanoparticles act as catalysts to (a) dissociate the precursor molecules and (b) provide nucleation sites for growth. This CVD process is sometimes also referred to as catalytic CVD (CCVD). There are clear similarities between CVD of nanowires and CNTs: in both cases, a catalyst particle dissociates and absorbs atoms from a gas-phase precursor and a second-phase, 1D nanomaterial is formed as the product (Moisala et al. 2003).

Depending upon the synthesis conditions, NWs are known to grow by two mechanisms: vapor–liquid–solid (VLS) or vapor–solid–solid (VSS) (Dasgupta et al. 2014). For VLS growth, the temperature is between the elemental melting point of the catalyst (1064 °C for Au) and the eutectic temperature (363 °C for Au–Si) such that the catalyst particle is initially solid (Fig. 7.1, stage 1). In the case of the Au–Si system, introducing Si-containing gas molecules (or reaction with a clean Si substrate) increases the concentration of dissolved Si in the Au particle. As the Si concentration in the Au particle increases and shifts isothermally to the Si-rich side of the phase diagram, it crosses the Au-rich liquidus line and the catalyst melts completely (Fig. 7.1, stage 2); eventually, the composition will reach the Si-rich liquidus line and solid Si precipitates (Fig. 7.1, stage 3). Continued dissociation and absorption of the Si into the liquid Au–Si alloy catalyst feeds continued NW growth (Fig. 7.1, stage 4). Fundamental aspects of NW and whisker growth via the VLS mechanism are reviewed in (Ross 2010; Bootsma and Gassen 1971; Givargizov 1975).

On the other hand, NW nucleation and growth via the VSS mechanism occurs from supersaturated solid particles below the eutectic temperature, where both the matrix and growing phase remain solid. The mechanism of NW growth is therefore simple precipitation, but with the important feature that the metal nanoparticles provide a template for growth and may control the diameter of the NW. Reference

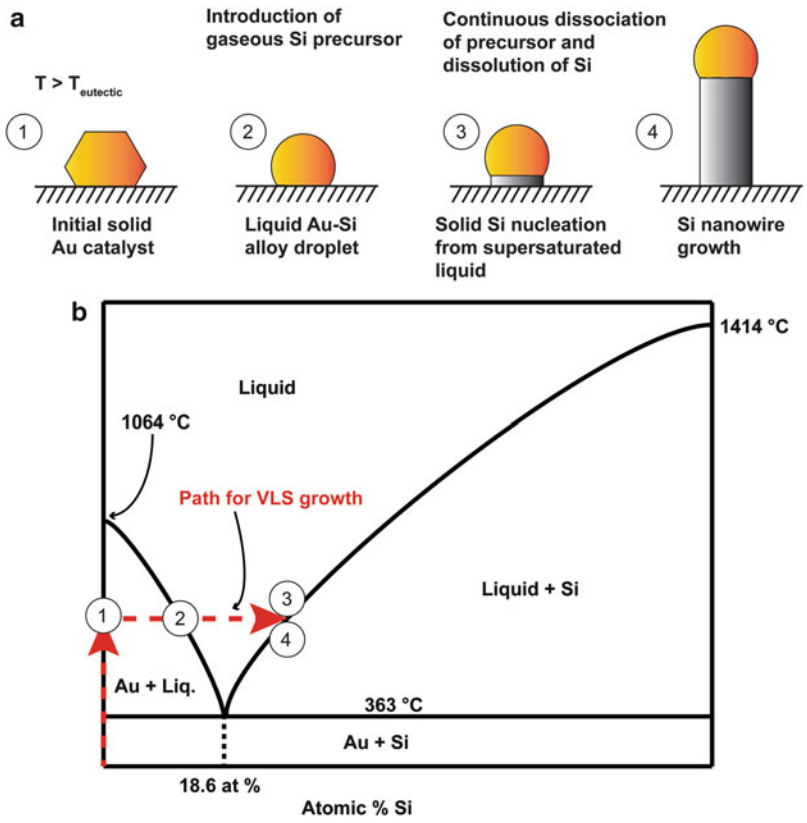

Fig. 7.1 (**a**) A schematic drawing showing the steps in growth of a Si nanowire via the VLS method and (**b**) the Au–Si phase diagram. The locations on the phase diagram corresponding to steps 1–4 in the schematic are labelled. The initially solid catalyst dissolves Si until melting completely (point 2). Once the Si concentration reaches the saturation level (point 3), the NW nucleates and grows. The phase diagram was redrawn based on information from Okamoto and Massalski (1983)

to a phase diagram is useful to understand the thermodynamics of VLS or VSS growth.

Compound semiconductor NWs are more complicated and require additional considerations as they are generally synthesized by metal organic CVD (MOCVD) process and require two or more precursor gases. Therefore, a ternary phase diagram is necessary to describe the possible phase transformations. For example, GaN NWs form by nitridation of liquid Au–Ga by ammonia (NH_3). Therefore, the composition of Au–Ga droplet has to be in the liquid region as identified in the Au–Ga phase diagram (Fig. 7.2a) and confirmed by experimental data shown in Fig. 7.2b, c (Diaz et al. 2012).

The most commonly reported gases used for NW growth are digermane and disilane for Ge and Si NWs, respectively. In situ measurements of GaN NW

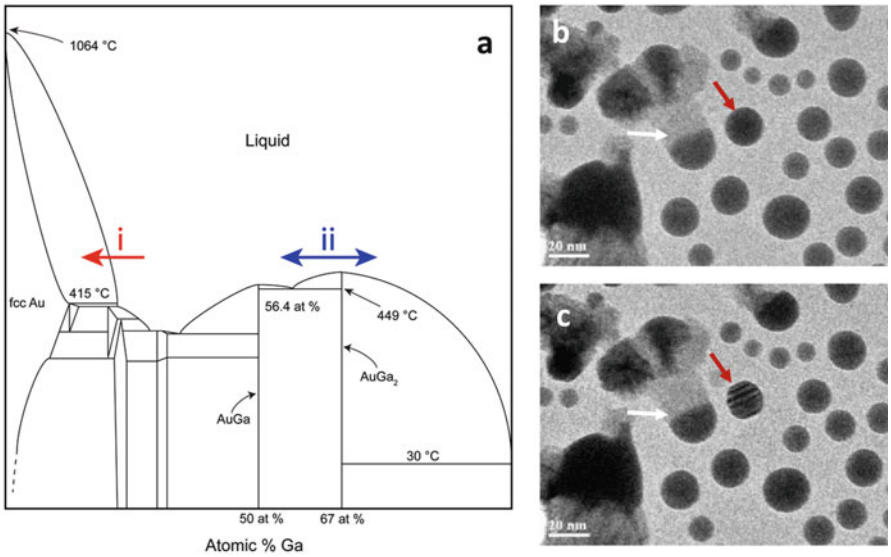

Fig. 7.2 (**a**) Au–Ga phase diagram. (**b**, **c**) time-resolved video frames recorded during GaN NW growth from Au–Ga liquid particles at 800 °C in 200 PaNH_3. *Red arrows* indicate step (i) where a liquid Au–Ga particle becomes Au rich, and thereby solid, after losing some Ga to the environment due to evaporation. *White arrows* indicate the NW growth if the particle composition is Ga rich, step (ii) in the phase diagram; the particle remains liquid

growth, using trimethylgallium (TMG) and ammonia (NH_3) have also been reported (Diaz et al. 2012). Although Au is the most commonly studied catalyst, other catalyst materials for semiconductor NW growth are also possible including Ag (Wittemann et al. 2010), Al (Wacaser et al. 2009), Ni (Purushothaman and Jeganathan 2013), Pd (Hofmann et al. 2008), Cu (Wen et al. 2009b), and alloys of these metals (Chou et al. 2012; Wen et al. 2009a; Gamalski et al. 2013; Robertson 2012).

The precise mechanisms of CVD CNT growth are still an active subject of research. Briefly, the process involves dissociation of the carbon-containing gas and the carbon adsorption on the catalyst surface, diffusion of the C atoms on the surface or in the bulk, formation of a CNT nucleus on the particle and CNT liftoff and growth. Questions remain about the chemical phase of the catalyst particle during growth, the role of bulk versus surface diffusion of C, the influence of particle size on CNT growth, and the initial nucleation and formation of a graphene layer on the catalyst particle prior to growth of the nanotube. It is likely that the details will vary significantly with growth conditions and metal catalyst used. In situ ETEM has shed light on a number of these questions as described in Sect. 7.8.2.

7.3 Advantages of In Situ Experiments

Ex situ, post-growth evaluation of nanomaterials in the TEM is a critically useful technique for understanding lattice defects, chemistry, etc. at high spatial resolution. However, it suffers from a number of limitations alleviated by direct in situ observations in the TEM. In particular, during cooling from the reaction temperature the catalyst particles may change phase, nanowires and nanotubes may change their morphology, etc. In the case of Si NW growth, Ross et al. showed sawtooth faceting on NW walls related to the presence of oxygen, and it appears that this faceting is often not observed ex situ due to changes during cooling after reaction (Ross et al. 2005). Another key advantage of in situ growth is the ability to directly measure growth rates of multiple individual nanomaterials in the same experiment. This capability has been exploited to identify time-dependent fluctuations in CNT growth (Sharma 2009) and to examine size effects in nucleation and growth of NWs (Kim et al. 2008; Kodambaka et al. 2006b).

7.4 Instrumentation Required

ETEM provides the most suitable platform for in situ growth studies as the chamber surrounding the sample can be used as a "cold wall" CVD reactor, allowing the complete set of nanoscale characterization techniques to be maintained. CVD growth studies require: (1) the ability to heat the sample (typically to temperatures in the range of ≈300 °C to ≈800 °C); and (2) the ability to introduce gas into the sample area. In an ideal situation, heating and gas introduction would occur rapidly and introduce negligible sample vibration and drift. Despite many years of effort and significant progress towards this goal, drift, and vibrations, nonetheless remain problems. The microscope design is described in more detail in Chap. 2 of this book and previously in several reviews (Sharma 2001; Boyes and Gai 1997; Hansen et al. 2010; Wagner et al. 2012) and heating holders are described in Chaps. 2 and 6, and will not be discussed here.

For gas introduction into the vacuum of the microscope column, differentially pumped systems with a gas inlet are now a commonly used design. In addition, UHV TEMs, with or without additional differential pumping, with gas-introduction hardware have been developed by a few researchers (Hammar et al. 1996; McDonald et al. 1989). The modified UHV systems start with a TEM capable of reaching base pressures below 1×10^{-7} Pa and are modified to introduce small amounts of gas (1×10^{-5} Pa) (Hammar et al. 1996; McDonald et al. 1989). One advantage of UHV systems is that by maintaining very low partial pressures of oxygen or water, reactions on clean surfaces, can be observed. For example, the effect of a low partial pressure of oxygen (~1×10^{-5} Pa) on Si NW growth was revealed using a UHV TEM (Ross 2010; Kodambaka et al. 2006a).

7.5 Experimental Design

When designing an in situ growth experiment, it is essential to consider what measures are necessary to ensure safe handling and use of the gases involved. Gas-handling systems and microscope use must be designed around safe operation in the same manner as a CVD reactor. Possible damage to the internal parts of the microscope must also be considered in the selection of reaction gases. For example, corrosive gases such H_2S and SO_2 Cl_2 should be avoided. Also, gas leak rates should be kept to a minimum level for disilane which can form silicon oxide coatings on internal microscope surfaces including apertures and vacuum pump components if the leak rate or pressure is too high.

A number of conditions for the gas-handling system must be met for successful nanomaterial growth. Both NW and CNT growth require a clean environment with very low partial pressures of water and other contaminants which can interfere with the primary catalytic reaction. Tubing on the gas-handling system should be bakeable so that water can be driven from the internal surfaces. The cleanliness of the setup is further discussed in Chap. 2.

The reaction condition (nature of gas and/or temperature) must also be compatible with the heating holders used. For example, Ta-based furnace holders should not be used with oxygen environments (Diaz et al. 2012). In addition, the grid and support materials must be carefully chosen. When using a furnace holder, metal evaporated from the grid can interact with catalyst particles (Zhang and Su 2009).

The next step in experimental design for nanomaterial growth should be checking the relevant equilibrium phase diagrams to identify possible phase transformations and the conditions necessary for growth. For example, the Au–Si phase diagram (Fig. 7.1) was used as a guide to identify VLS growth conditions for Si nanowire growth. A similar strategy was also used to determine VLS and VSS growth conditions for Ge NW and Si NW growth using Au and Pd as catalysts, respectively (Hofmann et al. 2008).

It is important to note that phase diagrams only provide information on thermodynamic equilibrium: kinetic effects must also be considered. Generally, this requires reviewing the in situ and ex situ literature for the reactions of interest. Important data to obtain include rates of gas decomposition as a function of temperature and pressure, diffusion constants, etc. It is also worth noting that nanoscale size effects can modify the stability of phases compared to what is expected from the bulk equilibrium phase diagram (Gamalski et al. 2010). The examples provided in Sect. 7.8 can be used as a guide to design ETEM experiments for similar systems.

7.6 Specimen Preparation Considerations

Specimen preparation for nanowire growth requires the creation of catalyst nanoparticles, such as Au, on a substrate. Evaporation or sputtering of metal films onto a substrate can produce the required particles for growth, where the density

and diameter of metal nanoparticles formed can be controlled by film thickness (see, e.g., Daudin et al. 2012)

In some ultra-high vacuum (UHV) TEMs, thin-film deposition is possible via evaporation within the UHV system (i.e., thin films can be deposited and samples inserted into the microscope without breaking vacuum) (Hammar et al. 1996; Ross 2010). For example, Au films of 1–2 nm thickness evaporated onto cleaned Si(111) substrates dewet in UHV to form small metal nanoparticles. The substrates were oriented so that the NWs grow perpendicular to the electron beam, a convenient geometry to image catalyst-NW interfaces and measure growth rates (Ross 2010).

Specimen preparation for CNT growth experiments must also be carefully designed to avoid certain pitfalls. Small particles (1–10 nm) are typically necessary for CNT growth and therefore the particle–substrate system must be chosen so that sintering via coalescence or Ostwald ripening of the particles does not occur at the reaction temperatures used. In the past, researchers have had success with NiO/SiO_x powder (Sharma and Iqbal 2004; Hofmann et al. 2007), $Fe–Al_2O_3$ (Amama et al. 2010), $NiO/MgAl_2O_4$ (Helveg et al. 2004), and Co–Mo/MgO (Sharma and Iqbal 2004; Picher et al. 2014). Sputtered or evaporated films may not always dewet the substrate properly to form small nanoparticles unless the combination of film and substrate is correctly chosen. In addition to the potential for particle size increase at high temperature, it has been shown that diffusion of catalyst material into the substrate can deactivate CNT growth (Kim et al. 2010b). Further discussion of catalyst–substrate interactions relevant to CNT growth in the ETEM is given by Kim et al. (2010a). One method for precise control of catalyst particle size, shape, and location is the deposition of particles in situ using electron-beam-induced deposition (EBID) (Sharma et al. 2009; Chee and Sharma 2012).

Typically, for transition metals, the nanoparticles are highly reactive and oxidize. Therefore, the particles and films are present as an oxide phase at room temperature and must be reduced to the metallic phase prior to CNT growth. Helveg et al. reduced NiO catalyst nanoparticles in ~100 Pa H_2 prior to CNT growth (Helveg et al. 2004). However, this step is not necessary as some of the C precursor gases such as acetylene or CO also act as reducing agents and have been reported to reduce iron, cobalt, and nickel oxides to the metal during the same reaction step as the growth. In fact, maintaining the nanoparticles in the oxide phase until the C precursor gas is introduced may be beneficial due to reduced sintering rates for the oxide compared to the metal nanoparticles during heating.

7.7 Data Analysis

Many software packages are available for analysis of videos or image stacks. In addition to commercial software, free and open-source software suitable for scientific analysis of time series is available, the best known of which is ImageJ (Schneider et al. 2012) (or its offshoot FIJI, Schindelin et al. 2012). Standard features of ImageJ include algorithms for thresholding, quantitative particle size

analysis, FFTs, Fourier filtering, etc. Multiple plugins are also available for spatial alignment of image stacks for this platform.

The ability to extract the growth rates of individual nanowires or nanotubes from in situ data is a key advantage of ETEM experiments. With such data in hand, it is possible to deduce the growth kinetics and identify the rate-limiting steps for the growth process and activation energies for various reactions. The general method is described by Sharma (2009) and consists of measuring growth rates at different temperatures and obtaining an Arrhenius plot to determine the activation energy. Details can be found in the relevant articles, (especially, Kim et al. 2008; Hofmann et al. 2008) and examples of kinetic information extracted from in situ measurements can be found in Sect. 7.8.

Measuring growth rates for individual CNTs is complicated due to their tubular structure and varying inner and outer diameters, thus requiring very careful analysis. For example, for a given outer tube diameter, it is not always possible to determine the number of walls, and therefore it is difficult or impossible to relate linear growth rates to the number of carbon atoms which have been incorporated into the tube and therefore it is not always possible to measure the activation energies for growth (Sharma 2009). This restriction does not apply to SWNTs or for imaging conditions which permit determination of the number of walls.

7.8 Examples of Information Gained from In Situ 1D Nanomaterial Growth Experiments

7.8.1 Nanowire Growth

The VLS mechanism had been proposed in the 1960s for growth of whiskers (Wagner and Ellis 1964), but had not been experimentally confirmed until recently. Early in situ TEM observations of Ge nanowire growth from Au catalysts were the first direct evidence of the VLS growth mechanism for nanowires (Wu and Yang 2001). In this set of experiments, the vapor source was solid material deposited on a TEM grid. Subsequent ETEM experiments using a gas-phase precursor confirmed the VLS mechanism for NW growth (Hannon et al. 2006). In situ microscopy is critical to verify if the catalyst particle is liquid during growth.

Application of semiconductor nanowires requires detailed knowledge of the parameters controlling the growth rate to permit dimensional control during fabrication and in situ ETEM offers the ability to make highly accurate measurements of the growth rates of individual NWs. The unique capabilities of UHV-ETEM have been exploited to measure the growth rates of individual NWs as their diameters tapered during growth. Theoretical predictions have suggested that the growth rate should decrease with nanowire diameter, but these direct measurements of Si NW growth rates for a range of sizes indicate that growth conditions, i.e., pressure and temperature, and not the size, affects the growth rate (Kodambaka et al. 2006b).

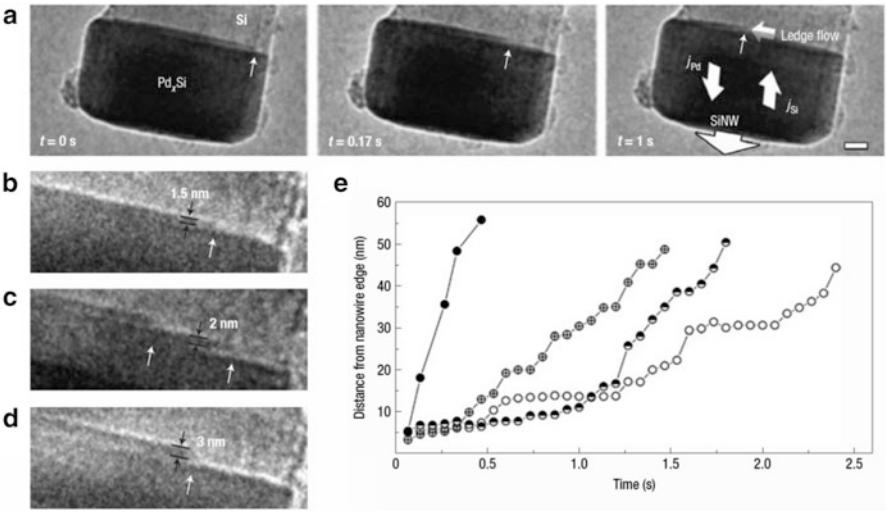

Fig. 7.3 (**a**) Sequence of images showing the growth of a Si NW from a Pd_xSi catalyst with time (t) (scale bar 10 nm), (**b–d**) various ledge configurations at the Pd_xSi/Si NW interface during growth, (**e**) measured step edge position with time for independent ledges

Another important contribution of in situ ETEM was the demonstration that the catalyst can be solid during NW growth (Kodambaka et al. 2007). Subsequent experiments have shown VSS growth in other systems such as Si NW growth from Pd and Cu catalysts (Hofmann et al. 2008; Wen et al. 2009b). These studies also revealed the existence of a ledge-flow controlled growth mechanism in which atomic-scale ledges at the interface between the solid catalyst and the nanowire move laterally resulting in the nanowire growth (see Fig. 7.3).

The nucleation rate dependence on the catalyst particle size was first reported by Hofmann et al. (2008). Direct in situ observation, using ETEM, revealed that smaller particles supersaturated, and thereby nucleated NWs, before larger particles as shown in Fig. 7.4. Incubation time for Si NW nucleation was measured to be $\propto A_o^{1/2}$, where A_o is the initial cross-sectional area of the Au particle.

They also showed that Si NWs grow via the VSS mechanism when using Pd as a catalyst. Their analysis of growth rates of Si NW growth from Pd_2Si catalysts allowed the rate-limiting step to be inferred (Hofmann et al. 2008). The activation energy and NW growth rates were inconsistent with a rate-limiting step set by an interfacial reaction. Instead, the data indicated that Pd diffusion away from the Si NW/silicide interface controlled the growth.

Useful kinetic and thermodynamic information extracted from in situ observations of individual NW nucleation and growth events also includes the quantification of the nucleation events for Si NWs (Kim et al. 2008). By quantifying the growth rate of Si crystals within multiple Au–Si liquid droplets at 585 °C, the authors were able to extract the activation energies for disilane dissociation and Si atoms joining the Si crystal from the liquid. A detailed study of the data obtained

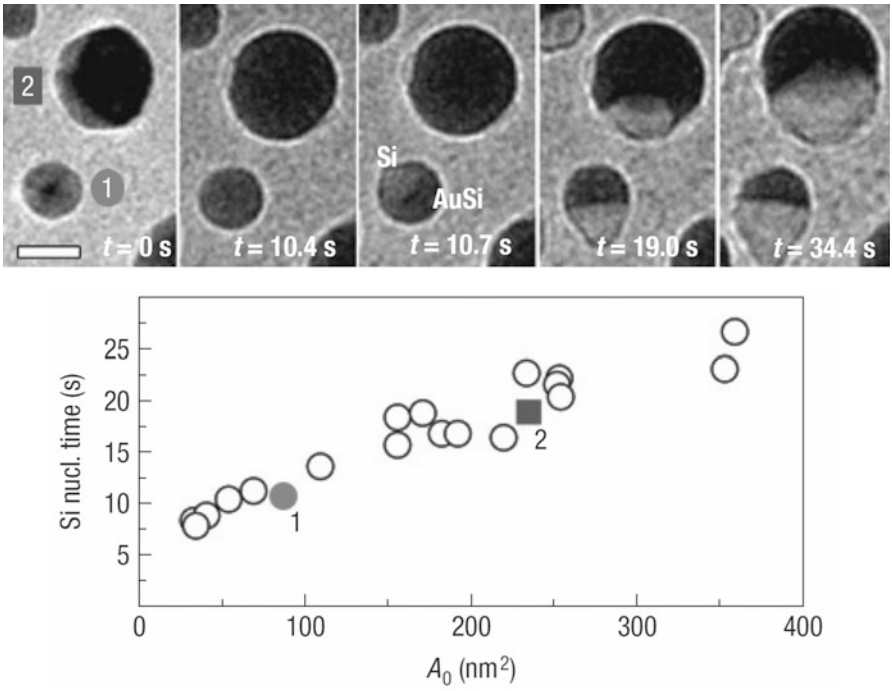

Fig. 7.4 ETEM images of the nucleation of Si NWs from Au catalysts (Hofmann et al. 2008). Analysis of multiple nucleation events indicates a size effect for nucleation. Nucleation occurs first in small Au catalyst particles

enabled many more conclusions to be drawn about the physical nature of the nucleation process (Kim et al. 2008).

An additional interesting phenomenon identified by in situ observations is the hysteresis in the state of the Au catalyst during Ge nanowire growth as a function of temperature, Ge_2H_6 pressure, and size. The catalyst particles at the tip of the growing NWs remain liquid below the eutectic temperature before solidifying abruptly. The solidification occurred as the temperature was lowered below the eutectic (undercooling) and the catalyst composition became Ge rich (Kodambaka et al. 2007). Upon reheating, catalyst particles melted at temperatures (superheating) above the eutectic point. The extent of undercooling or superheating was also observed to be dependent on the Ge_2H_6 pressure, i.e., the dissociative adsorption rate in Au particles. As a result, NWs were observed to grow both by VLS and VSS under the same growth conditions (Kodambaka et al. 2007).

ETEM growth experiments have also revealed fundamental features of growth that influence NW morphology and the introduction of defects such as kinks. ETEM was used to identify temperature regimes that produced straight or "wormy" NW growth (Fig. 7.5) (Madras et al. 2009). In particular, Si NWs that started out straight at 425 °C became kinked when the temperature was reduced to 380 °C. Real-time imaging of Si NW kinking was obtained, showing a transition in growth directions

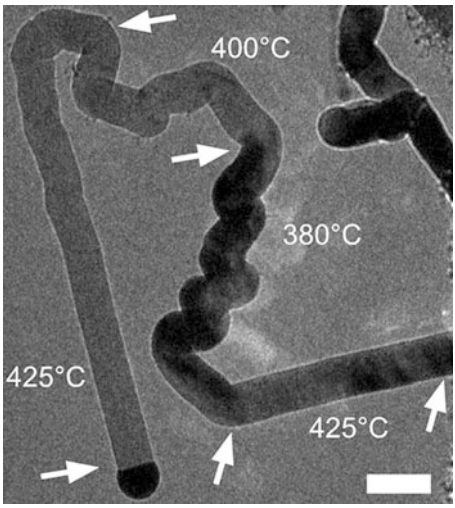

Fig. 7.5 Image of a Si NW after growth showing the changes in morphology as the growth temperature is varied. Higher growth temperatures produce straighter, unkinked NWs. Scale bar is 250 nm. Reprinted with permission from (Madras et al. 2009), Copyright 2009 American Chemical Society

between equivalent <111> directions or from <111> to <112> directions. Figure 7.5 shows an image after in situ growth where a single NW has grown straight in some regions and kinked at other points depending on the temperature, which was varied during the growth experiment. The disilane pressure also influenced the growth morphology (Madras et al. 2009).

Other research using ETEM has related kinking behavior to changes in the dimensions of the NW (Hillerich et al. 2013). If the NW diameter shrinks, an inclined facet can form and the NW can continue growing outward from the new facet (Hillerich et al. 2013). Such effects are especially prominent for hybrid structures, where a new material is grown on top of another material and the change in interfacial energies can induce NW diameter changes. Another source of NW diameter change is out-diffusion of Au from the catalyst causing shrinkage of the catalyst particle. Au diffusion is sensitive to the reaction conditions used such as oxygen partial pressure (Hannon et al. 2006; Kodambaka et al. 2006a). Au out-diffusion during growth of Si NWs introduces several other phenomena revealed by in situ ETEM experiments. For example, as Au diffuses along the NW surface the Si surface energy is modified, causing the introduction of "saw-tooth" faceting (Ross et al. 2005). Ostwald ripening of catalyst particles occurs as Au diffuses from the smaller to the larger particles, leading to changes in catalyst size during growth (Kodambaka et al. 2006a). ETEM also revealed that the presence of a small amount of oxygen in the reaction chamber prevented Au diffusion on the NW side walls (Kodambaka et al. 2006a).

While the majority of investigations of NW growth have focused on semiconductors grown from a catalyst material, metal oxide nanowires can be grown directly by a reaction of the metal with oxygen gas. Recently, Rackauskas et al. observed the growth mechanisms of CuO NWs, in situ, by exposure of Cu metal to oxygen in the ETEM (Rackauskas et al. 2014).

7.8.2 CNT Growth

In situ observations of carbon nanotube (CNT) growth in the TEM possibly extends back to the earliest days of gas–cell microscopy in the TEM when Baker and Harris obtained images of carbon filaments in a modified TEM (Baker and Harris 1972; Baker 1989). The low-resolution in situ images obtained did not clearly show the filaments to be CNTs. High-resolution images and diffraction patterns, collected post-growth, show amorphous carbon filaments as well as thick graphitic layers in some filaments indicating that their structure may be similar to multi-wall CNTs. These filaments were of interest as they were identified as a potential source of catalyst poisoning and deactivation for hydrocarbon cracking reactions. Baker et al. also presented a growth model based on carbon supersaturated particles that was widely accepted until recently (Baker et al. 1972).

ETEM observations from multiple groups have shown that the catalyst particle remains solid during CNT growth (Hofmann et al. 2009), clarifying the controversy regarding the possibility of growth from a liquid particle (Harutyunyan et al. 2005; Cantoro et al. 2006) due to proposed significant melting point depression for nanoparticles at growth temperatures. Ex situ TEM data could not, of course, confirm the state of the particle during growth. During in situ ETEM observation of carbon nanofiber (CNF) growth from Ni particles the catalyst remained solid while undergoing huge deformations which could be explained by rapid solid-state diffusion at the growth temperatures (Hofmann et al. 2007).

During the last couple of decades, unprecedented results have been obtained by direct imaging of CNT nucleation and growth process at reaction temperature using ETEM (Helveg et al. 2004; Zhu et al. 2005; Hofmann et al. 2007). Helveg et al. were also first to show that surface diffusion of carbon and not bulk diffusion is a prominent feature for CNT growth (Helveg et al. 2004). Later, Sharma and Iqbal employed ETEM to identify reaction temperatures that produced different types of CNTs using catalysts of NiO/SiO_x and Co–Mo/MgO and acetylene as the precursor (Sharma and Iqbal 2004).

Even without atomic-resolution imaging of CNT growth, ETEM experiments enable precise measurement of the growth rates of individual tubes, adding to the understanding of catalyst poisoning and growth mechanisms. Early work showed different growth regimes for a single CNT over time and eventually the slowing and end of growth even though the temperature and gas pressure were not changed (Lin et al. 2006).

Only within the last decade, with the development of higher-resolution ETEMs, has it been possible to reveal the atomic-level growth mechanisms of CNTs on catalyst particles (Helveg et al. 2004; Zhu et al. 2005; Hofmann et al. 2007). Pioneering work by several groups has provided clear evidence of a number of features of CNT growth. For example, Yoshida et al., showed that Fe catalyst particles during CNT growth are transformed to the cementite phase Fe_3C, as

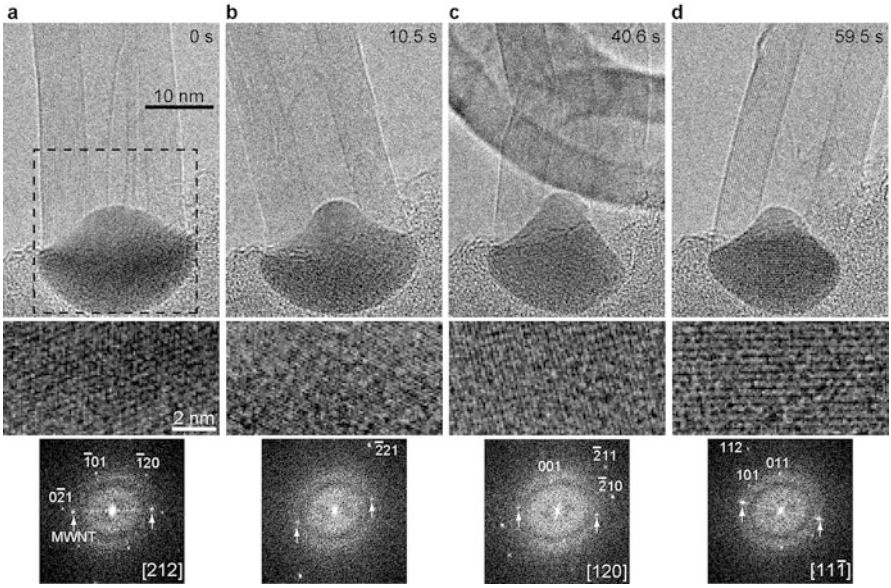

Fig. 7.6 (**a**-**d**) Low magnification in situ ETEM images during CNT growth from a Fe catalyst (*top row*). Analysis of FFTs (*bottom row*) from the lattice fringes (*middle row*) indicates the active phase during growth is cementite

illustrated in Fig. 7.6 (Yoshida et al. 2008) or a more complex Mo-containing carbide in the presence of Mo (Yoshida et al. 2012). Together with other observations, this information strongly suggested that bulk diffusion occurs during CNT growth from Fe catalysts because the entire catalyst particle adopted the observed carbide structure (Yoshida et al. 2008). Recently, the crystal structures of active and inactive particles have been identified by examining a number of HRTEM images of Fe catalysts, recorded under reaction conditions, during CNT growth and after growth termination. Experimental data show that the structure of active particles is cementite (Fe_3C) and that of inactive particles is Hägg phase (Fe_5C_2) (Mazzucco et al. 2014). In situ evidence in fact indicated that termination of CNT growth was correlated with the formation of the Hägg phase. Density functional theory (DFT) calculations further confirmed that the inactivity of the Fe_5C_2 structure is due to the lower mobility of the C atoms and the higher C–C bond formation energies on the stable (010) surface (Mazzucco et al. 2014).

The unexpected restructuring and shape changes of a solid catalyst particle, a liquid-like behavior, during CNT growth were first observed by ETEM. It was known from ex situ TEM imaging that metal particles could be incorporated into the hollow center of the nanotube (Ajayan et al. 1994), but the mechanism of incorporation was unclear. Direct in situ evidence of a Ni catalyst particle changing shape during tip growth of a nanofiber was obtained by Helveg et al. (2004) who showed elongation and contraction of the Ni catalyst. Restructuring during the

initial stages of growth was also observed for a Ni catalyst during root growth (Hofmann et al. 2007).

The driving force for the catalyst particle reshaping during growth and becoming incorporated within the CNT is still open to debate. Interpretations based on capillary forces, strong metal-carbon bonding, etc. have been proposed (Sun et al. 2006; Schebarchov and Hendy 2008). Molecular dynamics (MD) simulations and continuum modeling have been shown to reproduce observations from ETEM experiments in work reported by Moseler et al. (2010). This study indicated that enhanced diffusion of Ni interface atoms and capillary forces could explain experimental observations. It was not necessary to assume that the Ni metal particle liquefied, instead the particle remained crystalline during MD simulations as the restructuring happened. This restructuring after nucleation identifies one of the limitations of controlling CNT growth by control of the initial catalyst particle features as new crystal facets can form and the particle size can change. Shape changes of the catalyst particle during growth were observed to be associated with the formation of the so-called bamboo structures during growth in an ETEM experiment (Lin et al. 2007).

The nucleation of an SWCNT on a catalyst particle has been the subject of much research because of the importance of this step in determining the SWCNT chirality. Ex situ TEM images, diffraction patterns, and lattice-energy-based theoretical simulations suggest that the atomic arrangement of the catalyst particle surface determines the structure of the SWCNT cap (and thereby the chirality) at the nucleation stage (Reich et al. 2006; Zhu et al. 2008; Koziol et al. 2010; Picher et al. 2014). However, the nucleation period is very short and difficult to capture during ETEM observations at the typical ~30 Hz frame rates of most charge-couple device (CCD) cameras. In addition, high resolution is necessary to observe the single atomic layer of C forming the nucleus, requiring high stability from the heating holder during the beginning of the reaction. Recently, Picher et al. have reported the formation of a graphene layer that developed into an SWCNT on a Co–carbide catalyst on an MgO support (Picher et al. 2014). Time-resolved images of the nucleation step were obtained by reducing the rate of SWCNT growth. In this work, an initial graphene layer was reported to form on a (020) facet of the Co_2C particle and remained tethered to one facet as the other edge of the graphene moved stepwise across a C-terminated (210) facet until reaching and attaching to another (020) surface, at which point the CNT grew out from the particle (Fig. 7.7). DFT calculations confirmed that different works of adhesion of graphene layer for the different crystallographic surfaces determined the tethering and lift-off facets for SWCNT on the catalyst nanoparticle (Picher et al. 2014).

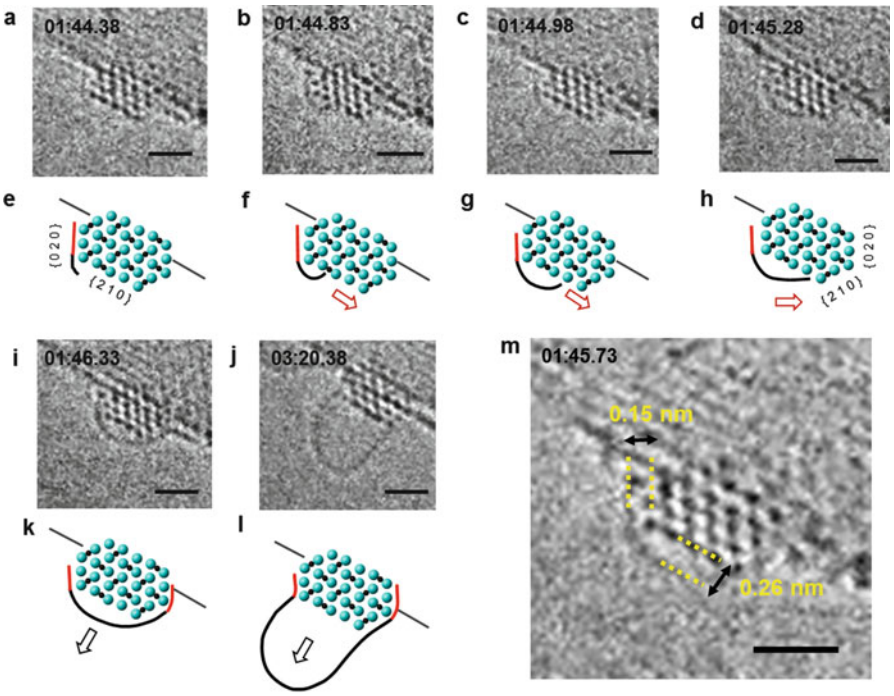

Fig. 7.7 (**a**–**d**, **i**, **j**) A series of images extracted from a video showing SWCNT growth from Co_2C nanoparticle. (**e**–**h**, **k**, **l**) Corresponding atomic models. The *red lines* indicate the stronger adhesion between graphene and metal on the two $Co_2C(020)$ surfaces and the *black line* shows slightly lifted graphene from {210} surface that results in the formation of cap, with the *arrows* indicating the SWCNT growth direction. (**m**) Snapshot showing the average distances between the growing structure and the {020} and {210} catalyst surfaces before the nanotube lift-off. Scale bars are 1 nm

7.9 Limitations

7.9.1 Electron Beam Damage

Various types of damage or other unwanted effects of electron beam irradiation can occur during in situ TEM imaging. Electron beam damage can be categorized into three main classes: (1) beam heating, (2) atom displacement and removal, and (3) contamination. Atom displacement can occur through one of several mechanisms depending on the material. It is important to keep in mind when considering radiation damage that, although the beam energy may be hundreds of thousands of electron volts, damage requires a mechanism for energy transfer from the beam electrons to the sample and higher beam energies can lead to less damage if the likelihood of the damage mechanism decreases. Ionization damage is reduced at higher voltages because the cross section for ionization decreases.

Energy absorbed in the specimen via inelastic scattering from the incident beam can heat the sample. The amount of energy deposited depends on the cross section for excitations, nature, and thickness of sample material. The important conditions to avoid are a high current in a small diameter beam with a low thermal conductivity support. A discussion of beam heating and an equation to calculate the temperature increase can be found in Egerton et al. (2004).

Perhaps the most serious result of beam irradiation for nanomaterial growth is contamination. Particularly for CNT growth, the presence of water and unwanted hydrocarbons on the sample or in the sample area can easily ruin an in situ experiment. Some recommendations for limiting contamination include: plasma clean the sample and support film when possible (Isabell et al. 1999) (carbon films can withstand short durations in a plasma cleaner of ~5 to 20 s); (McGilvery et al. 2012) avoid the use of acetone as cleaning agent or to disperse the catalyst particles on TEM grids—instead use ethanol or isopropanol of high purity from a glass container or use dry loading; heat the sample and film in a clean or inert atmosphere (heating in argon was used to clean graphene films attached to lacey carbon on copper grids for nano-area diffraction) (Tendeloo et al. 2012).

In addition to build-up of material on the sample, contaminant molecules can cause sample etching. The presence of water in particular can catalyze the etching of carbonaceous materials under the electron beam according to the following reactions which can convert C into CO and CO_2: (Hren et al. 1979).

$$H_2O \rightarrow H_2O^+ + e^-$$
$$H_2O^+ + C \rightarrow H + H^+ + CO$$

Ross has reported that the beam has little effect on growth kinetics as the NWs in unirradiated regions can be seen to be approximately the same length as NWs exposed to the beam. However, the beam can decompose the precursor gases causing deposition on the NW sidewalls (Ross 2010).

Carbon materials can be damaged by atom displacement by knock-on damage. The low atomic number of carbon means that the threshold for displacement is usually below the accelerating voltage used. To avoid atom displacement, a beam energy below ~80 kV should be used (Smith and Luzzi 2001). The results of atom displacements in CNTs include the reduction of the diameter as atoms are removed and the formation of a variety of defects. At elevated temperatures, carbon atoms are mobile in CNTs and radiation damage can cause unexpected changes in the CNTs including joining of separate CNTs (Banhart 2006).

Beam heating is expected to be negligible for CNTs as the small cross section for scattering and low thickness mean little energy is transferred to cause heating and CNTs have a high thermal conductivity that quickly removes deposited heat (Banhart 2006; Smith and Luzzi 2001). However, small nanoparticle catalysts on a thermally insulating substrate may experience some beam heating.

Under growth conditions, the anti-contamination device (cold finger) is not used, leading to the presence of a small amount of water that is particularly problematic for imaging of CNTs due to the catalytic etching effect described previously (Mølhave et al. 2007). If imaging of CNTs after growth is necessary, in the

experience of the authors, beam effects can be reduced if the sample temperature is kept at or above ~200 °C which reduces the absorption of water by the sample and allows the point defects generated by the beam to anneal.

Imaging of CNTs grown in the ETEM away from the electron beam shows that for a range of imaging and growth conditions the beam has no measurable effect as CNTs are similar in irradiated and non-irradiated regions after growth at high temperatures. However, the effect of electron radiation should always be monitored for every reaction condition.

7.9.2 Temperature Measurement

Although it had been previously recognized as a potential problem and studied to a limited extent (Baker and Harris 1972), the precise decrease in specimen temperature with gas introduction has not been measured until recently. Direct sample temperature measurements for flowing H_2 and N_2 have been made using diffraction to measure metal lattice expansion (Winterstein et al. 2014) and Raman scattering to measure changes in vibrational states (Picher et al. 2015). Temperature changes of several hundred degrees Celsius have been measured for pressures of ~100 Pa H_2. At much lower pressures (<10 Pa), the change in specimen temperature may be negligible, but it cannot be ignored for high ETEM pressures. Because the nature of nanomaterial growth is very sensitive to specimen temperature, it is important to consider the quenching effect of gases and several test runs may be necessary to identify proper conditions. This should be considered when trying to match in situ reaction conditions to ex situ results.

7.10 Future Research Directions

The features of 1D nanomaterial growth discovered by ETEM experiments confirms the value of ETEM for understanding the basic science of nanotube and nanowire growth. While ETEM experiments have answered many questions, new questions have arisen and remain to be resolved.

Looking to the future, we anticipate higher time resolution to study nucleation events and other rapid phenomena. Imaging with higher time resolution will require new cameras with frame rates greater than the typical ~30 Hz capabilities of CCDs and more stable holders to limit drift during fast heating. New, faster cameras and micro-electro-mechanical system (MEMS) holders with lower drift rates are now available and are being used (see Chap. 5). Detectors with higher quantum efficiencies, necessary for high-speed imaging, can also reduce dose requirements. New correlative techniques for more thorough analysis, e.g., combining light spectroscopy and TEM imaging, should enable a greater understanding of growth processes in the ETEM. Better control of sample temperature with the newer generation of MEMS-based holders should also permit greater accuracy in the extraction of kinetic and thermodynamic information.

References

P.M. Ajayan, C. Colliex, J.M. Lambert, P. Bernier, L. Barbedette, M. Tence, O. Stephan, Growth of manganese filled carbon nanofibers in the vapor phase. Phys. Rev. Lett. **72**(11), 1722–1725 (1994)

P.B. Amama, C.L. Pint, S.M. Kim, L. McJilton, K.G. Eyink, E.A. Stach, R.H. Hauge, B. Maruyama, Influence of alumina type on the evolution and activity of alumina-supported Fe catalysts in single-walled carbon nanotube carpet growth. ACS Nano **4**(2), 895–904 (2010). doi:10.1021/nn901700u

R.T.K. Baker, Catalytic growth of carbon filaments. Carbon **27**(3), 315–323 (1989). doi:http://dx.doi.org/10.1016/0008-6223(89)90062-6

R.T.K. Baker, P.S. Harris, Controlled atmosphere electron microscopy. J. Phys. E Sci. Instrum **5** (8), 793 (1972)

R.T.K. Baker, M.A. Barber, P.S. Harris, F.S. Feates, R.J. Waite, Nucleation and growth of carbon deposits from the nickel catalyzed decomposition of acetylene. J. Catal. **26**(1), 51–62 (1972). doi:10.1016/0021-9517(72)90032-2

F. Banhart, Irradiation of carbon nanotubes with a focused electron beam in the electron microscope. J. Mater. Sci. **41**(14), 4505–4511 (2006). doi:10.1007/s10853-006-0081-0

R.H. Baughman, A.A. Zakhidov, W.A. de Heer, Carbon nanotubes—the route toward applications. Science **297**(5582), 787–792 (2002). doi:10.1126/science.1060928

G.A. Bootsma, H.J. Gassen, A quantitative study on the growth of silicon whiskers from silane and germanium whiskers from germane. J. Cryst. Growth **10**(3), 223–234 (1971). doi:http://dx.doi.org/10.1016/0022-0248(71)90188-6

E.D. Boyes, P.L. Gai, Environmental high resolution electron microscopy and applications to chemical science. Ultramicroscopy **67**(1-4), 219–232 (1997). doi:10.1016/S0304-3991(96)00099-X

M. Cantoro, S. Hofmann, S. Pisana, V. Scardaci, A. Parvez, C. Ducati, A.C. Ferrari, A.M. Blackburn, K.-Y. Wang, J. Robertson, Catalytic chemical vapor deposition of single-wall carbon nanotubes at Low temperatures. Nano Lett. **6**(6), 1107–1112 (2006). doi:10.1021/nl060068y

C.K. Chan, H. Peng, G. Liu, K. McIlwrath, X.F. Zhang, R.A. Huggins, Y. Cui, High-performance lithium battery anodes using silicon nanowires. Nat. Nanotechnol. **3**(1), 31–35 (2008). doi:http://www.nature.com/nnano/journal/v3/n1/suppinfo/nnano.2007.411_S1.html

S.W. Chee, R. Sharma, Controlling the size and the activity of Fe particles for synthesis of carbon nanotubes. Micron **43**(11), 1181–1187 (2012). doi:http://dx.doi.org/10.1016/j.micron.2012.01.008

Y.-C. Chou, C.-Y. Wen, M.C. Reuter, D. Su, E.A. Stach, F.M. Ross, Controlling the growth of Si/Ge nanowires and heterojunctions using silver–gold alloy catalysts. ACS Nano **6**(7), 6407–6415 (2012). doi:10.1021/nn301978x

Y. Cui, Q. Wei, H. Park, C.M. Lieber, Nanowire nanosensors for highly sensitive and selective detection of biological and chemical species. Science **293**(5533), 1289–1292 (2001). doi:10.1126/science.1062711

N.P. Dasgupta, J. Sun, C. Liu, S. Brittman, S.C. Andrews, J. Lim, H. Gao, R. Yan, P. Yang, 25th Anniversary article: semiconductor nanowires—synthesis, characterization, and applications. Adv. Mater. **26**(14), 2137–2184 (2014). doi:10.1002/adma.201305929

R. Daudin, C. Revenant, G. Davi, G. Renaud, Growth and dewetting of gold on Si(111) investigated in situ by grazing incidence small angle x-ray scattering. Physica E Low Dimens. Syst. Nanostruct. **44**(9), 1905–1909 (2012). doi:http://dx.doi.org/10.1016/j.physe.2012.05.021

R.E. Diaz, R. Sharma, K. Jarvis, Q. Zhang, S. Mahajan, Direct observation of nucleation and early stages of growth of GaN nanowires. J. Cryst. Growth **341**(1), 1–6 (2012). doi:http://dx.doi.org/10.1016/j.jcrysgro.2011.09.028

M.S. Dresselhaus, G. Dresselhaus, P. Avouris, *Carbon Nanotubes: Synthesis, Structure, Properties, and Applications* (Springer, Berlin, 2001)

R.F. Egerton, P. Li, M. Malac, Radiation damage in the TEM and SEM. Micron **35**(6), 399–409 (2004). doi:10.1016/j.micron.2004.02.003

A.D. Gamalski, J. Tersoff, R. Sharma, C. Ducati, S. Hofmann, Formation of metastable liquid catalyst during subeutectic growth of germanium nanowires. Nano Lett. **10**, 2972–2976 (2010)

A.D. Gamalski, D.E. Perea, J. Yoo, N. Li, M.J. Olszta, R. Colby, D.K. Schreiber, C. Ducati, S.T. Picraux, S. Hofmann, Catalyst composition and impurity-dependent kinetics of nanowire heteroepitaxy. ACS Nano **7**(9), 7689–7697 (2013). doi:10.1021/nn402208p

E.I. Givargizov, Fundamental aspects of VLS growth. J. Cryst. Growth **31**, 20–30 (1975). doi:http://dx.doi.org/10.1016/0022-0248(75)90105-0

M. Hammar, F.K. LeGoues, J. Tersoff, M.C. Reuter, R.M. Tromp, *In situ* ultrahigh vacuum transmission electron microscopy studies of hetero-epitaxial growth I. Si(001)Ge. Surf. Sci. **349**(2), 129–144 (1996). doi:http://dx.doi.org/10.1016/0039-6028(95)01068-8

J.B. Hannon, S. Kodambaka, F.M. Ross, R.M. Tromp, The influence of the surface migration of gold on the growth of silicon nanowires. Nature **440**(7080), 69–71 (2006). doi:10.1038/nature04574

T. Hansen, J. Wagner, R. Dunin-Borkowski, Aberration corrected and monochromated environmental transmission electron microscopy: challenges and prospects for materials science. Mater. Sci. Technol. **26**(11), 1338–1344 (2010). doi:10.1179/026708310X12756557336355

A.R. Harutyunyan, T. Tokune, E. Mora, Liquid as a required catalyst phase for carbon single-walled nanotube growth. Appl. Phys. Lett. **87**(5), 87–89 (2005). doi:http://dx.doi.org/10.1063/1.2005395

S. Helveg, C. Lopez-Cartes, J. Sehested, P.L. Hansen, B.S. Clausen, J.R. Rostrup-Nielsen, F. Abild-Pedersen, J.K. Norskov, Atomic-scale imaging of carbon nanofibre growth. Nature **427**(6973), 426–429 (2004). doi:http://www.nature.com/nature/journal/v427/n6973/suppinfo/nature02278_S1.html

K. Hillerich, K.A. Dick, C.-Y. Wen, M.C. Reuter, S. Kodambaka, F.M. Ross, Strategies to control morphology in hybrid group III–V/group IV heterostructure nanowires. Nano Lett. **13**(3), 903–908 (2013). doi:10.1021/nl303660h

A.I. Hochbaum, P. Yang, Semiconductor nanowires for energy conversion. Chem. Rev. **110**(1), 527–546 (2009). doi:10.1021/cr900075v

S. Hofmann, R. Sharma, C. Ducati, G. Du, C. Mattevi, C. Cepek, M. Cantoro, S. Pisana, A. Parvez, F. Cervantes-Sodi, A.C. Ferrari, R. Dunin-Borkowski, S. Lizzit, L. Petaccia, A. Goldoni, J. Robertson, *In situ* observations of catalyst dynamics during surface-bound carbon nanotube nucleation. Nano Lett. **7**(3), 602–608 (2007). doi:10.1021/nl0624824

S. Hofmann, R. Sharma, C.T. Wirth, F. Cervantes-Sodi, C. Ducati, T. Kasama, R.E. Dunin-Borkowski, J. Drucker, P. Bennett, J. Robertson, Ledge-flow-controlled catalyst interface dynamics during Si nanowire growth. Nat. Mater. **7**(5), 372–375 (2008). doi:http://www.nature.com/nmat/journal/v7/n5/suppinfo/nmat2140_S1.html

S. Hofmann, R. Blume, C.T. Wirth, M. Cantoro, R. Sharma, C. Ducati, M. Hävecker, S. Zafeiratos, P. Schnoerch, A. Oestereich, D. Teschner, M. Albrecht, A. Knop-Gericke, R. Schlögl, J. Robertson, State of transition metal catalysts during carbon nanotube growth. J. Phys. Chem. C **113**(5), 1648–1656 (2009). doi:10.1021/jp808560p

J.J. Hren, J. Goldstein, D.C. Joy, *Introduction to Analytical Electron Microscopy* (Plenum Press, New York, 1979)

S. Iijima, Helical microtubules of graphitic carbon. Nature **354**(6348), 56–58 (1991)

T.C. Isabell, P.E. Fischione, C. O'Keefe, M.U. Guruz, V.P. Dravid, Plasma cleaning and its applications for electron microscopy. Microsc. Microanal. **5**(02), 126–135 (1999). doi:10.1017/S1431927699000094

B.J. Kim, J. Tersoff, S. Kodambaka, M.C. Reuter, E.A. Stach, F.M. Ross, Kinetics of individual nucleation events observed in nanoscale vapor-liquid-solid growth. Science **322**(5904), 1070–1073 (2008). doi:10.1126/science.1163494

S.M. Kim, C.L. Pint, P.B. Amama, R.H. Hauge, B. Maruyama, E.A. Stach, Catalyst and catalyst support morphology evolution in single-walled carbon nanotube supergrowth: growth

deceleration and termination. J. Mater. Res. **25**(10), 1875–1885 (2010a). doi:10.1557/JMR.2010.0264

S.M. Kim, C.L. Pint, P.B. Amama, D.N. Zakharov, R.H. Hauge, B. Maruyama, E.A. Stach, Evolution in catalyst morphology leads to carbon nanotube growth termination. J. Phys. Chem. Lett. **1**(6), 918–922 (2010b). doi:10.1021/jz9004762

S. Kodambaka, J.B. Hannon, R.M. Tromp, F.M. Ross, Control of Si nanowire growth by oxygen. Nano Lett. **6**(6), 1292–1296 (2006a). doi:10.1021/nl060059p

S. Kodambaka, J. Tersoff, M.C. Reuter, F.M. Ross, Diameter-independent kinetics in the vapor-liquid-solid growth of Si nanowires. Phys. Rev. Lett. **96**(9), 096105 (2006b)

S. Kodambaka, J. Tersoff, M.C. Reuter, F.M. Ross, Germanium nanowire growth below the eutectic temperature. Science **316**(5825), 729–732 (2007). doi:10.1126/science.1139105

K.K.K. Koziol, C. Ducati, A.H. Windle, Carbon nanotubes with catalyst controlled chiral angle. Chem. Mater. **22**(17), 4904–4911 (2010). doi:10.1021/cm100916m

M. Lin, J.P. Ying Tan, C. Boothroyd, K.P. Loh, E.S. Tok, Y.-L. Foo, Direct observation of single-walled carbon nanotube growth at the atomistic scale. Nano Lett. **6**(3), 449–452 (2006). doi:10.1021/nl052356k

M. Lin, J.P.Y. Tan, C. Boothroyd, K.P. Loh, E.S. Tok, Y.-L. Foo, Dynamical observation of bamboo-like carbon nanotube growth. Nano Lett. **7**(8), 2234–2238 (2007). doi:10.1021/nl070681x

P. Madras, E. Dailey, J. Drucker, Kinetically induced kinking of vapor−liquid−solid grown epitaxial Si nanowires. Nano Lett. **9**(11), 3826–3830 (2009). doi:10.1021/nl902013g

S. Mazzucco, Y. Wang, M. Tanase, M. Picher, K. Li, Z. Wu, S. Irle, R. Sharma, Direct evidence of active and inactive phases of Fe catalyst nanoparticles for carbon nanotube formation. J. Catal. **319**, 54–60 (2014). doi:http://dx.doi.org/10.1016/j.jcat.2014.07.023

M.L. McDonald, J.M. Gibson, F.C. Unterwald, Design of an ultrahigh-vacuum specimen environment for high-resolution transmission electron microscopy. Rev. Sci. Instrum. **60**(4), 700–707 (1989). doi:http://dx.doi.org/10.1063/1.1141004

C.M. McGilvery, A.E. Goode, M.S.P. Shaffer, D.W. McComb, Contamination of holey/lacey carbon films in STEM. Micron **43**(2–3), 450–455 (2012). doi:http://dx.doi.org/10.1016/j.micron.2011.10.026

M. Meyyappan, *Carbon Nanotubes: Science and Applications* (CRC Press, Boca Raton, 2005)

A. Moisala, A.G. Nasibulin, E.I. Kauppinen, The role of metal nanoparticles in the catalytic production of single-walled carbon nanotubes—a review. J. Phys. Condens. Matter **15**(42), S3011 (2003)

K. Mølhave, S.B. Gudnason, A.T. Pedersen, C.H. Clausen, A. Horsewell, P. Bøggild, Electron irradiation-induced destruction of carbon nanotubes in electron microscopes. Ultramicroscopy **108**(1), 52–57 (2007). doi:http://dx.doi.org/10.1016/j.ultramic.2007.03.001

M. Moseler, F. Cervantes-Sodi, S. Hofmann, G. Csányi, A.C. Ferrari, Dynamic catalyst restructuring during carbon nanotube growth. ACS Nano **4**(12), 7587–7595 (2010). doi:10.1021/nn102118y

H. Okamoto, T.B. Massalski, The Au−Si (Gold-Silicon) system. Bull. Alloy Phase Diagrams **4**(2), 190–198 (1983). doi:10.1007/BF02884878

M. Picher, P.A. Lin, J.L. Gomez-Ballesteros, P.B. Balbuena, R. Sharma, Nucleation of graphene and its conversion to single-walled carbon nanotubes. Nano Lett. (2014). doi:10.1021/nl501977b

M. Picher, S. Mazzucco, S. Blankenship, R. Sharma, M. Picher, S. Mazzucco, S. Mazzucco, Vibrational and optical spectroscopies integrated with environmental transmission electron microscopy. Ultramicroscopy **150**, 10–15 (2015). doi:10.1016/j.ultramic.2014.11.023

V. Purushothaman, K. Jeganathan, Investigations on the role of Ni-catalyst for the VLS growth of quasi-aligned GaN nanowires by chemical vapor deposition. J. Nanopart. Res **15**(7), 1–12 (2013). doi:10.1007/s11051-013-1789-9

S. Rackauskas, H. Jiang, J.B. Wagner, S.D. Shandakov, T.W. Hansen, E.I. Kauppinen, A.G. Nasibulin, *In situ* study of noncatalytic metal oxide nanowire growth. Nano Lett. **14** (10), 5810–5813 (2014). doi:10.1021/nl502687s

S. Reich, L. Li, J. Robertson, Control the chirality of carbon nanotubes by epitaxial growth. Chem. Phys. Lett **421**(4–6), 469–472 (2006). doi:http://dx.doi.org/10.1016/j.cplett.2006.01.110

M.E. Reimer, G. Bulgarini, N. Akopian, M. Hocevar, M.B. Bavinck, M.A. Verheijen, E.P.A.M. Bakkers, L.P. Kouwenhoven, V. Zwiller, Bright single-photon sources in bottom-up tailored nanowires. Nat. Commun. **3**, 737 (2012)

J. Robertson, Realistic applications of CNTs. Mater. Today **7**(10), 46–52 (2004). doi:http://dx.doi.org/10.1016/S1369-7021(04)00448-1

J. Robertson, Heterogeneous catalysis model of growth mechanisms of carbon nanotubes, graphene and silicon nanowires. J. Mater. Chem. **22**(37), 19858–19862 (2012). doi:10.1039/C2JM33732K

F.M. Ross, Controlling nanowire structures through real time growth studies. Rep. Prog. Phys. **73** (11), 114501 (2010)

F.M. Ross, J. Tersoff, M.C. Reuter, Sawtooth faceting in silicon nanowires. Phys. Rev. Lett. **95** (14), 146104 (2005)

D. Schebarchov, S.C. Hendy, Capillary absorption of metal nanodroplets by single-wall carbon nanotubes. Nano Lett. **8**(8), 2253–2257 (2008). doi:10.1021/nl080875s

J. Schindelin, I. Arganda-Carreras, E. Frise, V. Kaynig, M. Longair, T. Pietzsch, S. Preibisch, C. Rueden, S. Saalfeld, B. Schmid, J.-Y. Tinevez, D.J. White, V. Hartenstein, K. Eliceiri, P. Tomancak, A. Cardona, Fiji: an open-source platform for biological-image analysis. Nat. Methods **9**(7), 676–682 (2012). doi:http://www.nature.com/nmeth/journal/v9/n7/abs/nmeth.2019.html#supplementary-information

C.A. Schneider, W.S. Rasband, K.W. Eliceiri, NIH Image to ImageJ: 25 years of image analysis. Nat. Methods **9**(7), 671–675 (2012)

R. Sharma, Design and applications of environmental cell transmission electron microscope for *in situ* observations of gas–solid reactions. Microsc. Microanal. **7**(06), 494–506 (2001)

R. Sharma, An environmental transmission electron microscope for *in situ* synthesis and characterization of nanomaterials. J. Mater. Res. **20**(07), 1695–1707 (2005). doi:10.1557/JMR.2005.0241

R. Sharma, Kinetic measurements from *in situ* TEM observations. Microsc. Res. Tech. **72**(3), 144–152 (2009). doi:10.1002/jemt.20667

R. Sharma, Experimental set up for *in situ* transmission electron microscopy observations of chemical processes. Micron **43**(11), 1147–1155 (2012). doi:http://dx.doi.org/10.1016/j.micron.2012.01.007

R. Sharma, Z. Iqbal, *In situ* observations of carbon nanotube formation using environmental transmission electron microscopy. Appl. Phys. Lett. **84**(6), 990–992 (2004). doi:http://dx.doi.org/10.1063/1.1646465

B.W. Smith, D.E. Luzzi, Electron irradiation effects in single wall carbon nanotubes. J. Appl. Phys. **90**(7), 3509–3515 (2001). http://dx.doi.org/10.1063/1.1383020

B.W. Smith, D.E. Luzzi, Electron irradiation effects in single wall carbon nanotubes. J. Appl. Phys. **90**(7), 3509–3515 (2001). doi:10.1063/1.1383020

L. Sun, F. Banhart, A.V. Krasheninnikov, J.A. Rodríguez-Manzo, M. Terrones, P.M. Ajayan, Carbon nanotubes as high-pressure cylinders and nanoextruders. Science **312**(5777), 1199–1202 (2006). doi:10.1126/science.1124594

G.V. Tendeloo, D. Van Dyck, S.J. Pennycook, *Handbook of Nanoscopy* (Wiley-VCH, Weinheim, 2012)

B.A. Wacaser, M.C. Reuter, M.M. Khayyat, C.-Y. Wen, R. Haight, S. Guha, F.M. Ross, Growth system, structure, and doping of aluminum-seeded epitaxial silicon nanowires. Nano Lett. **9**(9), 3296–3301 (2009). doi:10.1021/nl9015792

R.S. Wagner, W.C. Ellis, Vapor-liquid-solid mechanism of single crystal growth. Appl. Phys. Lett. **4**(5), 89–90 (1964). doi:http://dx.doi.org/10.1063/1.1753975

J.B. Wagner, F. Cavalca, C.D. Damsgaard, L.D.L. Duchstein, T.W. Hansen, Exploring the environmental transmission electron microscope. Micron **43**(11), 1169–1175 (2012). doi: http://dx.doi.org/10.1016/j.micron.2012.02.008

D. Wang, A. Pierre, M.G. Kibria, K. Cui, X. Han, K.H. Bevan, H. Guo, S. Paradis, A.-R. Hakima, Z. Mi, Wafer-level photocatalytic water splitting on GaN nanowire arrays grown by molecular beam epitaxy. Nano Lett. **11**(6), 2353–2357 (2011). doi:10.1021/nl2006802

C.-Y. Wen, M.C. Reuter, J. Bruley, J. Tersoff, S. Kodambaka, E.A. Stach, F.M. Ross, Formation of compositionally abrupt axial heterojunctions in silicon-germanium nanowires. Science **326** (5957), 1247–1250 (2009a). doi:10.1126/science.1178606

C.Y. Wen, M.C. Reuter, J. Tersoff, E.A. Stach, F.M. Ross, Structure, growth kinetics, and ledge flow during vapor−solid−solid growth of copper-catalyzed silicon nanowires. Nano Lett. **10** (2), 514–519 (2009b). doi:10.1021/nl903362y

J. Winterstein, P. Ann Lin, R. Sharma, Measurement of local specimen temperature under flowing Gas ambient in the environmental scanning transmission electron microscope (ESTEM) using diffraction. Microsc. Microanal. **20**(S3), 1596–1597 (2014). doi:10.1017/S1431927614009714

J.V. Wittemann, W. Münchgesang, S. Senz, V. Schmidt, Silver catalyzed ultrathin silicon nanowires grown by low-temperature chemical-vapor-deposition. J. Appl. Phys. **107**(9), 096105 (2010). doi:http://dx.doi.org/10.1063/1.3393601

Y. Wu, P. Yang, Direct observation of vapor−liquid−solid nanowire growth. J. Am. Chem. Soc. **123**(13), 3165–3166 (2001). doi:10.1021/ja0059084

P. Yang, The chemistry and physics of semiconductor nanowires. MRS Bull **30**, 85–91 (2005)

H. Yoshida, S. Takeda, T. Uchiyama, H. Kohno, Y. Homma, Atomic-scale in-situ observation of carbon nanotube growth from solid state iron carbide nanoparticles. Nano Lett. **8**(7), 2082–2086 (2008). doi:10.1021/nl080452q

H. Yoshida, H. Kohno, S. Takeda, *In situ* structural analysis of crystalline Fe–Mo–C nanoparticle catalysts during the growth of carbon nanotubes. Micron **43**(11), 1176–1180 (2012). doi:http://dx.doi.org/10.1016/j.micron.2012.04.008

Z. Zhang, D. Su, Behaviour of TEM metal grids during in-situ heating experiments. Ultramicroscopy **109**(6), 766–774 (2009). doi:http://dx.doi.org/10.1016/j.ultramic.2009.01.015

H. Zhu, K. Suenaga, A. Hashimoto, K. Urita, K. Hata, S. Iijima, Atomic-resolution imaging of the nucleation points of single-walled carbon nanotubes. Small **1**(12), 1180–1183 (2005). doi:10.1002/smll.200500200

H. Zhu, K. Suenaga, J. Wei, K. Wang, D. Wu, A strategy to control the chirality of single-walled carbon nanotubes. J. Cryst. Growth **310**(24), 5473–5476 (2008). doi:http://dx.doi.org/10.1016/j.jcrysgro.2008.09.174